ELSEVIER

Int. J. Therm. Sci. 41 (2002) 229–240

International Journal of Thermal Sciences

www.elsevier.com/locate/ijts

Forced heat convection in a reciprocating duct fitted with 45 degree crossed ribs

Shyy Woei Chang

Department of Marine Engineering, National Kaohsiung Institute of Marine Technology, Kaohsiung, Post code: 811, Taiwan, ROC

Received 15 January 2001; accepted 4 April 2001

Abstract

This experimental study investigated heat-transfer physics of forced convection in a reciprocating square duct fitted with 45° crossed ribs on two opposite walls. The parametric conditions involved several Reynolds, pulsating and buoyancy numbers, respectively, in the ranges of 600–10 000, 0–10, and 0–0.14 with five different reciprocating frequencies tested, namely, 0.67, 1, 1.33, 1.67 and 2 Hz. The rib-induced flows in the static duct produced an augmentation of heat transfer in the range of 260–300% compared to the smooth-walled situation. The reciprocating heat-transfer data reconfirmed the appearance of large-scale wavy-like axial heat transfer distribution that differed significantly from the stationary results. The manner in which the pulsating force and convective inertia, with and without buoyancy interaction, interactively affected the local heat transfer along the rib-roughened surface was illustrated using a number of experimentally based observations and extrapolations. The buoyancy interaction in the reciprocating duct reduced heat transfer, which effect was enhanced by increasing the pulsating number, but appeared to be a weak function of Reynolds number. When the Reynolds and pulsating numbers were relatively low, a range of heat transfer impediments, that could lead the spatial-time averaged heat-transfer to levels about 71% of nonreciprocating values, was observed. A further increase of pulsating number resulted in a subsequent heat-transfer recovery, which tendency could lead to heat-transfer improvement from the nonreciprocating level. An empirical correlation to evaluate the spatial-time averaged heat transfer over the reciprocating ribbed duct was developed to assist the design activity. The possibility to further enhance heat-transfer via the use of angled ribs in a reciprocating duct is confirmed, but it is important to ensure that the range of reciprocating flow parameters produced does not create heat-transfer impediment in order to avoid overheating situations.

Keywords: Reciprocating heat convection; Skewed crossed ribs

1. Introduction

The development of low speed diesel engines for commercial ship propulsions in recent years pursues low fuel consumption and high propulsive efficiency. Under these design initiatives, the maximum cycle pressure and temperature of the engine reach about 125 bar and 1500 °C. The engine speed is reduced to the range of 90–115 rev/min by increasing the stroke-to-bore ratio so that the propulsive efficiency is improved. Heat transfer augmentation for the cooling system in the piston becomes essential in order to cope with the increased thermal loads. Fig. 1 illustrates two typical types of internal cooling systems in the piston. As shown for the Sulzer RTA90 engine, the coolant in the blind bores of piston crown has to transfer heat downward. Each blind bore in the piston acts as an anti-gravity open thermosyphon. The reciprocating force drives the coolant circulation in the tubular thermosyphon, which creates the heat transfer capability. In the cooling passages of piston crown for the B&W L90GB engine, the reciprocating motion of piston affects the forced convection of coolant flow. For further heat transfer augmentation, a various types of repeated ribs could be cast on the surfaces of these cooling channels.

Although the use of surface ribs has been a subject of much fundamental research over the years for stationary duct flow situations [1–5], only few research efforts investigate the flow and heat transfer in the ribbed channel when the flow pulsates as with the application to the piston cooling [6–9]. The effectiveness of surface ribs on the heat transfer augmentation depends on the geometrical factors of the ribs, such as the height, pitch, angle of attack, orientation, shape, arrangement [1–5], and on the external force-field present [5,

E-mail address: swchang@mail.nkimt.edu.tw (S.W. Chang).

1290-0729/02/$ – see front matter
PII: S1290-0729(01)01311-4

Nomenclature

a	smooth entry length	m
Bi	Biot number $= hl/k_w$	
Bu	Buoyancy number $= \beta(T_w - T_b)\omega^2 RdW_m^{-2}$	
C_p	specific heat of coolant	$J{\cdot}kg^{-1}{\cdot}K^{-1}$
d	hydraulic diameter of test duct	m
e	rib height	m
H	height of test duct	m
h	convective heat transfer coefficient	$W{\cdot}m^{-1}{\cdot}K^{-1}$
k	thermal conductivity of coolant	$W{\cdot}m^{-1}{\cdot}K^{-1}$
k_w	thermal conductivity of duct wall	$W{\cdot}m^{-1}{\cdot}K^{-1}$
L	land of rib	m
l	thickness of duct wall	m
Nu	reciprocating Nusselt number $= q_f d/(T_w - T_b)k_f$	
Nu_0	non-reciprocating Nusselt number	
Nu_∞	Nusselt number of developed flow in stationary smooth-walled duct	
P	pitch of ribs	m
Pu	Pulsating number $= \omega R/W_m$	
q_f	convective heat flux	$W{\cdot}m^{-2}$
R	reciprocating amplitude	m
Re	Reynolds number $= \rho W_m d/\mu$	
T_b	flow bulk temperature	K
T_w	wall temperature	K
W	width of test duct	m
W_m	mean through flow velocity	$m{\cdot}s^{-1}$
z	axial coordinate	m
Z	dimensionless axial location $= z/d$	

Greek symbols

β	thermal expansion coefficient of coolant	K^{-1}
ρ	coolant density	$kg{\cdot}m^{-3}$
μ	dynamic viscosity of coolant	$kg{\cdot}s^{-1}{\cdot}m^{-1}$
ω	angular velocity of rotating disc creating reciprocating motion	$rad{\cdot}s^{-1}$

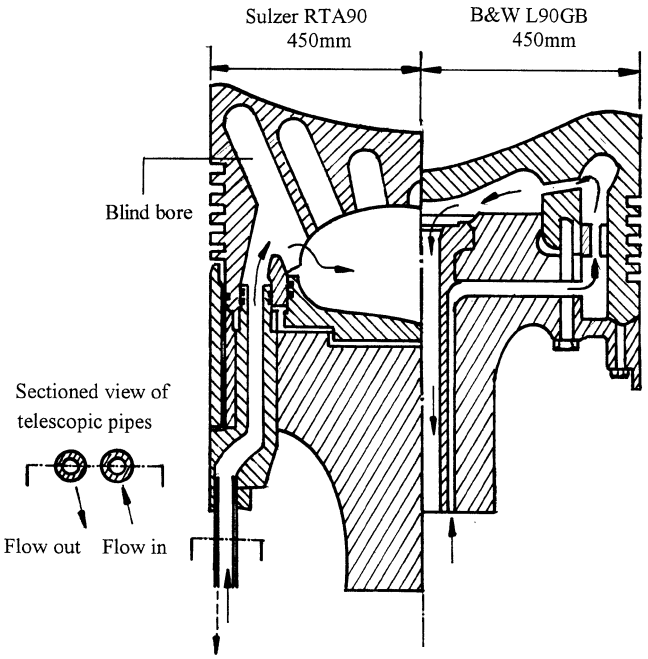

Fig. 1. Internal cooling networks of piston for Sulzer RTA90 and B&W L90GB Engines.

8–12]. These surface ribs enhance the turbulent fluctuations and could considerably modify the near-wall flow structures by creating the secondary flows and vortices. They penetrate the sublayers of flow to cause the periodic redevelopment of boundary layers. The overall rib-effects on heat transfer are the improved heat transmission and the modified spatial distributions. In [11], the stagnant vortices behind the 90° transverse ribs raise the fluid temperature in the re-circulating zone and the wall temperature near the rib location. Local heat transfer improvement develops near the reattaching point between ribs. When the flow traverses the staggered angled-ribs, the spanwise, counter-rotating, double-cell vertical secondary flows develop. These vortices move along the inclined surface ribs that induce the spanwise heat transfer variation on the ribbed wall. The locally high heat transfer rates on a ribbed surface develop at the locations where the fluid is relatively cool [2,11]. Between the 90°, 45°, V-shaped and discrete ribs, the 45° angled ribs show the highest thermal performance when the friction loss is considered [2]. However the other force field established in the ribbed duct flow, such as the centrifugal force in the bend [5] and the rotating or reciprocating force [8–12], could modify the rib-induced flows. The dynamic process with cancellation and enhancement of the rib-flows occurs in a ribbed channel when the mainstream oscillates or pulsates. In [7], the interaction of the oscillating mainstream with the angled-rib-flow triggers a double pair of dynamic counter-rotating vortical cells, with one attached on the angled rib while the other sheds away from the rib. The detailed growing and shedding process of these vortices depends on the oscillating frequency of mainstream, the attack angle of ribs and the maximum flow velocity. Even in the duct fitted with transverse ribs, the flow cells behind the 90° ribs are no longer stagnant but periodically varied when the duct reciprocates. The typical zigzag streamwise heat transfer variation along the ribbed wall in a stationary system yields into the large wavy pattern in the reciprocating duct [8]. These reciprocating effects must be fully understood if the reliable cooling performance of piston is to be predicted at the design stage.

The present paper describes the results of a series of experiments aimed at studying the effect of reciprocating motion on heat transfer in a square duct fitted with 45°

crossed ribs. The direction of reciprocating force is in parallel with the axial direction of the ribbed duct. This study forms part of the on-going research program into the heat transfer augmentation of reciprocating ducted-flow with reference to the piston cooling application. The study has two phases. Initially the stationary duct flow conditions are examined to generate the database to which the reciprocating results obtained at the second phase could be compared to assess the reciprocating effects on heat transfer.

2. Experimental details

2.1. Strategy

The primary tasks of the present study are to generate the heat transfer data in a reciprocating duct fitted with 45° angled ribs and to examine the combined effect of these periodic ribs and reciprocating motion on heat transfer. The translating velocity of test duct, motivated by the rigid slider-crank mechanism of a piston or by the present reciprocating facility, is not a constant value but a skewed sinusoidal function. When the length ratio of the connecting rod to the crank arm is greater than 8, the translating velocity of test duct can be approximated by $R\omega \sin \omega t$ [13]. Because the reciprocating test duct accelerates, the Galiean invariance, which requires the Navier–Stokes equations in a coordinate system translating with constant velocity to be the same as those in a stationary coordinate system, becomes invalid. A modified version of Navier–Stokes equations that considers the effect of translating acceleration of the coordinate system on the fluid motion is usually convenient to describe the dynamic mechanism of the governing forces involved in a reciprocating system. A study of the momentum conservation equations, with the fluid motion referred to a coordinate frame which reciprocates with the flow boundary itself, suggests that the fluid motion is governed parametrically by Reynolds (*Re*), pulsating (*Pu*) and reciprocating buoyancy (*Bu*) numbers [8]. The pulsating number, *Pu*, and buoyancy number, *Bu*, respectively, quantify the ratio of pulsating to inertial forces and the relative strength of the reciprocating buoyancy effect [8]. When the temperature variation of coolant did not make a considerable change of coolant's Prandtl number, the local Nusselt number (*Nu*) could be parametrically described by the following equation

$$Nu = \phi\{Re, Pu, Bu, \text{ Boundary conditions}\} \quad (1)$$

All the dimensionless groups appearing in Eq. (1) are defined in the nomenclature section and ϕ is an, as yet, unknown function. The strategic aim of the present study is to identify the physics of heat transfer in association with the individual and combined effects of the non-dimensional groups appearing in Eq. (1). In the limiting case of a condition having a vanishing small wall-to-fluid temperature difference but the test duct reciprocates, the heat transfer function ϕ in Eq. (1) shall reflect the combined *Re* and *Pu* effects without any buoyancy interaction. As a real fluid has non-zero β value, it is not feasible to conduct a heat transfer experiment at the zero buoyancy condition. Thus the zero buoyancy effect has to be inferred by extrapolating a family of heat transfer data taken at a specific Reynolds or pulsating number with different wall-to-fluid temperature difference. In other words, the tests conducted at different heat flux levels will be extrapolated to the zero buoyancy asymptote ($\beta(T_w - T_b) = 0$, $\omega \neq 0$). For a set of boundary conditions simulated by the heat transfer test module, such as the geometrical features of ribbed duct, heating condition, and flow entrance, the effects of those constituent dimensionless groups indicated in Eq. (1) are examined by systematically varying each of the flow parameters involved in Eq. (1). A subsequent data reduction program follows the definitions of the dimensionless groups shown in Eq. (1), which generates the non-dimensional raw data for further analysis.

2.2. Test model and data reduction

The heat transfer test module shown in Fig. 2 was vertically installed onto a reciprocating facility that created the reciprocating motion of test duct. The schematics of the reciprocating facilities have been previously reported [8]. As shown in Fig. 2, the square sectioned test duct (1) fitted with fifteen pairs of square-shaped 45° angled ribs at a regular downstream interval was made of the bronze copper plate having a thermal conductivity of 50 $W \cdot m^{-1} \cdot K^{-1}$ at temperature 20 °C. The 1.5 mm thick square duct was 225 mm long. Hydraulic diameter of the test duct was 15 mm. The angled ribs on the two opposite walls were arranged in the cross manner so that the rib orientations on the two opposite walls were, respectively, positive and negative. Geometric features of the test section were specified in terms of five non-dimensional groups defined in Fig. 2 as:

- Smooth entry length/hydraulic diameter ratio $(a/d) = 0.5$;
- Rib height/hydraulic diameter ratio $(e/d) = 0.1$;
- Pitch/rib height ratio $(P/d) = 10$;
- Land/pitch ratio $(L/P) = 0.1$;
- Aspect ratio of test duct $(H/W) = 1$.

The coolant, water, flowed through a 1250 mm long smooth-walled square duct prior to entering the ribbed section (1). Along the surface fitted with the positive angled ribs, twenty equal-spaced type *K* thermocouples (2) were embedded into the duct wall. The actual distance of each thermocouple bead from the inner smooth-walled surface was 0.5 mm. The axial positions of these thermocouples corresponded to the first ten ribs and midribs locations. The representative wall temperature, T_w, was estimated from the thermocouple measurement using the one-dimensional conduction correction to the value of inner smooth wall. Because the effect of three-dimensional wall-conduction in the ribbed wall contaminated this 1-D correction, especially for

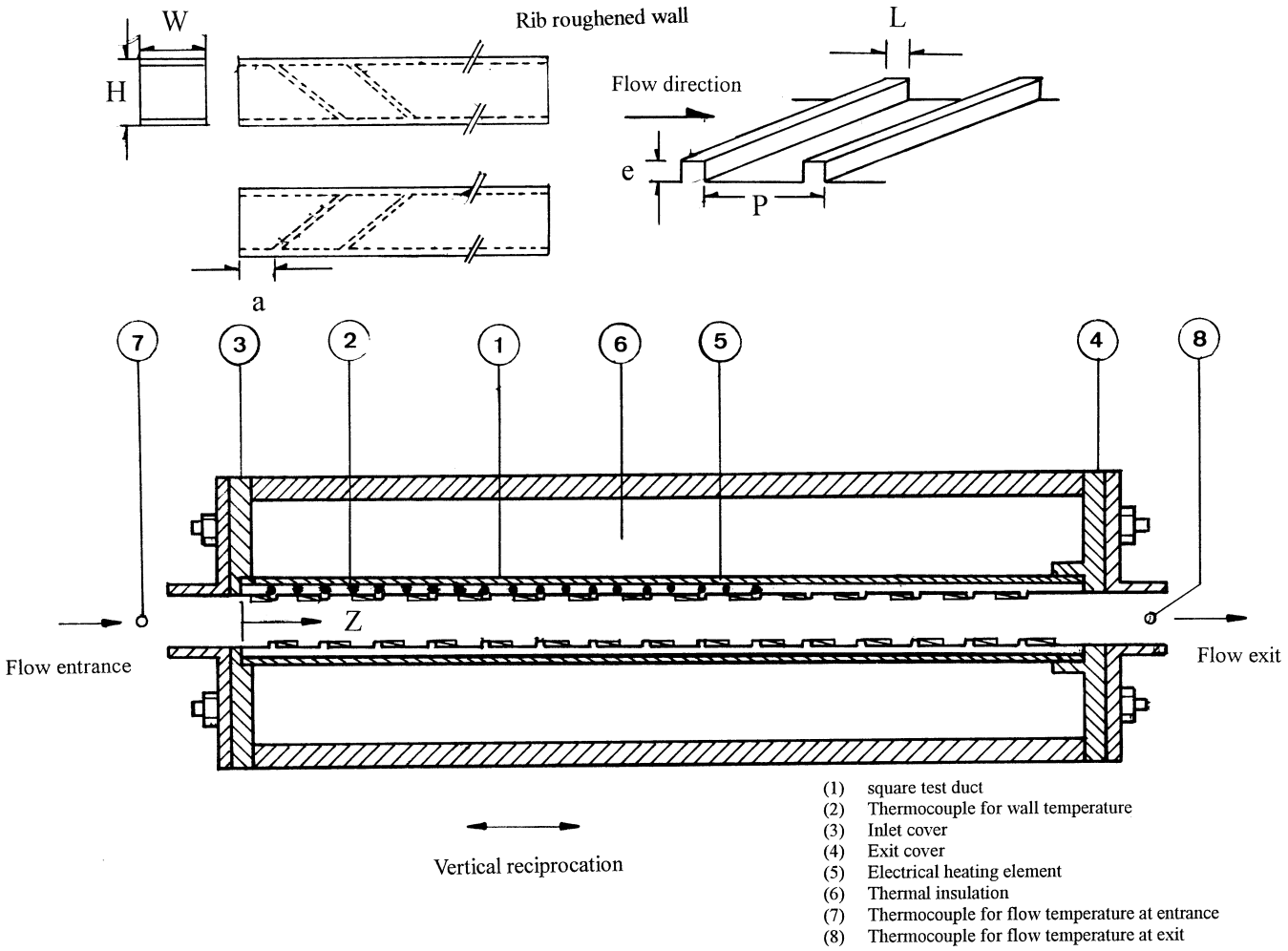

Fig. 2. Heat transfer test module.

the measurement at the rib location, the data collected from the rib location was disregarded from this presentation. Furthermore, as the flow field is unsteady that results in the periodical temperature variations on the inner surface of reciprocating duct, the heat conduction and heat capacity components of the wall could damp out the temperature oscillation if the measurement is made at the thermocouple location. A review of the heat transfer data generated form the present test-matrix showed that the range of Biot numbers (*Bi*) tested were well less than 0.1, which enabled the use of lumped transient conduction model [14] to examine such wall conduction effect on the temperature measurement. The theoretical solution of this transient conduction model revealed that the amplitude of temperature oscillation measured with a distance away from the fluid-wall interface could be alleviated. However, the measurement of time-mean temperature by the thermocouple was not changed from the value at the fluid-wall interface if the flow reached a quasi-steady state. Thus, in what follows, only the time-averaged data at each mid-rib location was analyzed and examined.

Two end-covers (3)(4) were made of Teflon to hold the test duct (1). Four long threads tightened the complete heat transfer assembly. On the outer surfaces of test duct (1), four thermal foils (5) were attached to provide the basically uniform heat flux heating condition. An adjustable power supply unit that allowed control of the heating power provided the required heating current. Adjusting the heating power supply varies the relative strength of the overall buoyancy level at any fixed flow condition. Thermal insulating material (6) was wrapped around the heated test section to minimize the external heat loss. For tests at the highest temperature settings and reciprocating frequency, the estimate heat loss during the experiment was about 8.9% of the total heating power supply. Two additional thermocouples (7)(8) penetrated into the core of the flow path to measure the fluid temperatures at entry and exit planes to the measurement section. All the temperature measurements were monitored and stored on a DX 33 PC through a Trend-Link Fluke Hydra 2620A-100 data logger for subsequent data processing.

In calculating the Nusselt number, the local fluid bulk temperature, T_b, was selected to define the wall-to-fluid temperature difference. Due to the difficulty of measuring fluid bulk temperatures inside the test duct without disturbing the flow field, the fluid temperature measured at the flow entrance was used as the starting reference for a sequential

integration of the local enthalpy to calculate the intermediate values of fluid bulk mean temperatures. Even in the time-dependent system when the test duct reciprocated, the local fluid bulk mean temperatures were defined by the same method of sequential integration of the local enthalpy. The net convective heat, q_f, used for calculating the local enthalpy balance and Nusselt number was obtained by subtracting the external heat loss and wall conductive heat from the total heating flux. The heat loss was evaluated based on the results from a series of heat loss calibration runs. The measured wall temperature distribution was numerically interpolated and a simple finite-difference representation of the Fourier conduction law was used to estimate the net wall conductive heat. To verify this calculating process, the calculated exit flow bulk temperature and the measurement detected by thermocouple (8) at the exit plane were compared for each data batch generated. The differences between the calculated exit flow bulk temperatures and measurements were within ±8%. The local coolant properties such as ρ, C_p, k, and μ were then evaluated by means of standard polynomial functions with the calculated fluid temperature as the determined variable. The nominal through flow Reynolds number was controlled by adjusting the mass flow rate measured at 150 diameters upstream of the test duct (1). Because the coolant properties, such as viscosity and density, varied with the local fluid temperature, the mass flow rate was adjusted to compensate the fluid-property variations in order to maintain the variations of Reynolds and pulsating numbers at the flow entrance within ±1% of the nominal values. These mass flow rate measurements along with the local fluid properties were incorporated with other measurements such as the reciprocating frequency to calculate the local non-dimensional groups in Eq. (1).

2.3. Program

The experimental program involved two phases. Initially the instrumentation and data reduction program were checked out with a series of baseline heat transfer experiments with a stationary test duct. This was followed by a series of reciprocating experiments, which data was compared with the baseline result to examine the individual and combined effects of *Re*, *Pu* and *Bu* on heat transfer. Two different sets of data were generated from the reciprocating experiments. The first set of reciprocating data was produced at fixed Reynolds numbers. At each fixed Reynolds number, five sets of tests at the reciprocating frequencies of 0.67, 1, 1.33, 1.67 and 2 Hz were performed. The data generated in this manner revealed the effect of pulsating number on heat transfer. The other set of experiments fixed the pulsating numbers at 2, 4, 6, 8 and 10 by adjusting the reciprocating frequency. At each fixed pulsating number, the flow conditions with five ascending Reynolds numbers were examined to reveal the Reynolds number effect. Note that the reciprocating frequencies were accordingly increased when the Reynolds numbers increased in order to control the pulsating number at a fixed value. At each selected Reynolds/pulsating number, five different levels of heating power, which heated the wall temperature at a downstream location of 5 tube diameters to levels of 40, 50, 60, 70 and 80 °C, respectively, were used to vary the buoyancy level systematically. This wall-temperature range was selected to avoid the local boiling. For each individual test, the flow and heating level were fixed for about 30 min in order to assure that the flow reached the quasi-steady state. Once such a flow state was reached, the on-line data acquisition system collected and stored the instantaneous data for a period of 10 seconds. These data were subsequently time-averaged and processed into the dimensionless groups defined in Eq. (1), with the fluid properties calculated from the local flow bulk temperature, which was determined using the method of local enthalpy balance. The parametric ranges in terms of Reynolds number, pulsating number, and buoyancy number were 600–10 000, 0–10 and 0–0.14, respectively. The range of Reynolds numbers selected was intended to cover both laminar and turbulent flow regimes. However, although the Reynolds number of 2300 has been well established to classify the laminar and turbulent flows in a static smooth-walled duct, the periodic ribs and reciprocating motion of test duct could modify the critical Reynolds number for transition. Thus the flow conditions tested with Reynolds numbers less than 2300 were characterized as the "low" Reynolds number tests, while the "high" Reynolds number tests referred to the flow conditions with $Re > 3000$.

An uncertainty approximation of the data reduction was conducted [15]. Because the quasi-steady state of the reciprocating flow system was approximated when variations of the local time-averaged wall temperatures were in the range of ±0.5 °C, the maximum uncertainty in temperature measurement was estimated to be ±0.5 °C. The maximum percentages of errors for the coolant's specific heat, mass flow rate and thermal conductivity, the fluid density, the hydraulic diameter of test duct, and the heating area were estimated as ±0.6%, ±6.8%, ±0.5%, ±0.3%, ±0.6%, and ±1.5%, respectively. With the temperature difference between the wall and fluid varied from 11 to 58 °C, the maximum uncertainty for the Nusselt, Reynolds, pulsating and buoyancy numbers were about 17%, 6%, 2%, and 5.3%, respectively.

3. Results and discussion

3.1. Nonreciprocating results

In order to reveal the heat transfer augmentation provided by the periodical angled ribs, the present stationary heat transfer data, Nu_0, was normalized by the developed Nusselt number value over the smooth-walled duct, Nu_∞. The selection of heat transfer reference, Nu_∞, has to consider the corresponding flow regime in a static smooth-walled duct. For low Reynolds numbers tested ($Re < 2300$), Nu_∞ was

selected as 3.63 [16], and this value was the developed heat transfer level in a square empty duct heated with uniform heat flux. With $Re > 3000$ (high Reynolds number range), the Dittus–Boelter value [17] was used to normalize Nu_0. The axial variations of the normalized Nusselt numbers, Nu_0/Nu_∞, at the mid-rib locations with flows in the low and high *Re* ranges are collected in Fig. 3(a) and (b), which, respectively, show the relative Nusselt number ratios of about 3 and 2.6. This heat transfer enhancement ratio decreases in the direction of flow from the inlet station, and tends to reach a constant value in the developed flow regions ($Z > 4$). Because the flow was developed hydraulically in the 1250 mm straight calming section before entering the heated section, this axial distribution was consistent with the development of the thermal boundary layer. The relative Nusselt number data shown in Fig. 3(a) for low Reynolds numbers tested collapses into a narrow data scatter band at each axial location. This indicates the weak dependence of heat transfer augmentation on the Reynolds number. With high Reynolds numbers tested, the Nusselt number ratios, Nu_0/Nu_∞, shown in Fig. 3(b) decreases with increase in the Reynolds number at all axial locations. This is felt to reflect the reduced Reynolds number exponent in the Nusselt number correlation for ribbed duct flow from 0.8 value in the Dittus–Boelter correlation [17]. Also shown, for comparative purposes, in Fig. 3(b) is the experimental data

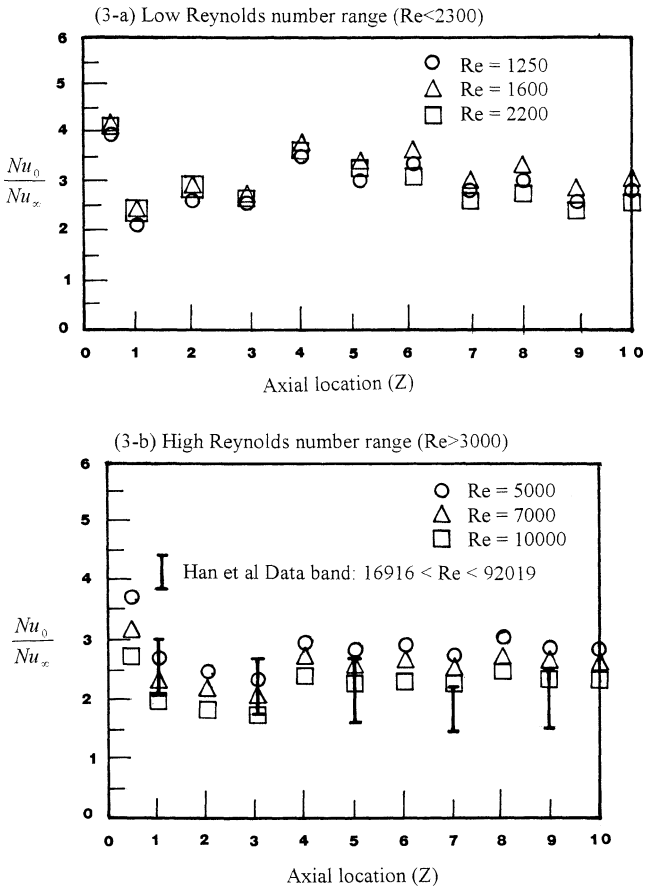

Fig. 3. Axial heat transfer distributions in static duct.

of Han et al. [1]. Good agreement between the present data and that of Han et al. [1] is evident. For the low and high Reynolds numbers examined in the static duct, the results obtained with different heater powers were collapsed into a negligible data scatter band. Therefore the buoyancy effect in the stationary duct was negligible.

3.2. Reciprocating results

When the test duct is reciprocated, the pulsating flow and oscillating pressure wave are induced within the test duct in which the rib-induced secondary flow cells develop. Accompanying this possibility of pulsation of the bulk flow is the modifications of the dynamic vortical flow cells, the turbulence structure, and the vorticity itself. This produces the attendant temporal Nusselt number variation at each measured station. Nevertheless, after taking the averaged value of the timewise Nusselt number data for a period of 10 seconds, the time-averaged heat transfer results along the ribbed wall were determined. Because we are dealing with a real fluid it is not possible to entirely eliminate buoyancy, and examine the combined effect of *Re* and *Pu* in isolation is not possible. However, in order to attempt this, comparisons of the *Re–Pu* coupling effect are made for tests where the spatially averaged values of buoyancy parameter, $\beta(T_w - T_b)$, are the same. With various static and reciprocating tests, the heat flux is adjusted to control the wall temperature at the predetermined values for the axial spot of $5Z$. Therefore, a heat transfer impediment on the reciprocating surface from the static level is reflected by a reduction of heat flux that causes the decrease of bulk mean fluid temperature, T_b, and consequently increases the respective wall-to-fluid temperature difference. This experimental approach is different with the theoretical study performed by Siegel [18] in which the heat transfer coefficients in a uniformly heated channel are compared at a fixed heat flux for different oscillating conditions. This manner of comparison revealed that the oscillation-induced axial energy flow could produce a significant increase in wall temperature from the static level, thereby producing a reduction of heat transfer when the oscillations are added to a steady flow [18]. When the duct walls are uniformly heated, the bulk mean fluid temperature, T_b, rises linearly along the channel length. Fig. 4(a) and (b), respectively, show the axial variations of the time-averaged Nusselt numbers with flows in the low and high Reynolds number regimes at a reciprocating frequency of 0.67 Hz. As shown, the increase of Reynolds number at a fixed reciprocating frequency reduces the pulsating number, and causes the heat transfer increment due to the increased mass flow rate. The worth noting observation is the development of large wavy-like axial heat transfer variation along the ribbed surface shown in Fig. 4(b). This “peak-valley”-like heat transfer distribution with a regular “wavelength” of two pitches along the ribbed surface is in consistent with the results found in a reciprocating square duct fitted with transverse ribs [8]. But this wavy-like distributing pattern

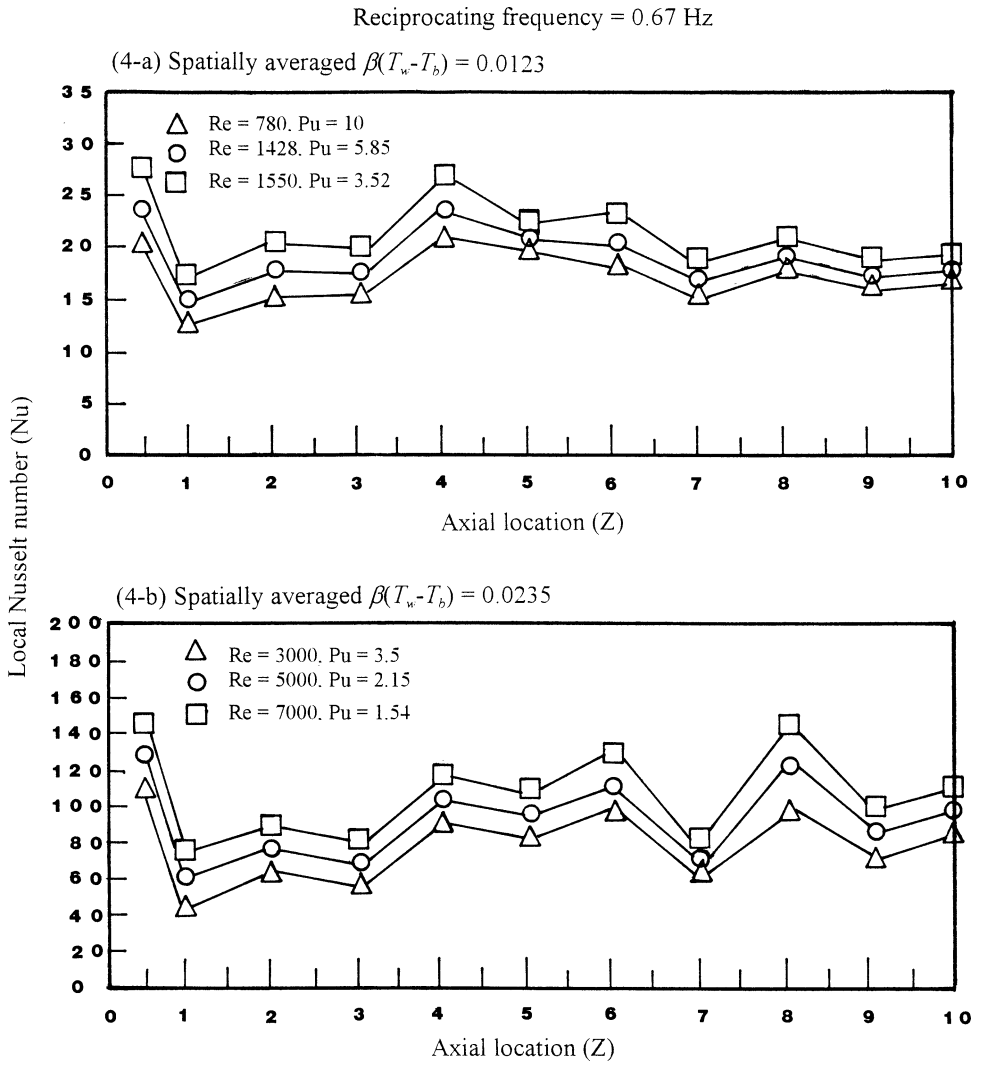

Fig. 4. Axial reciprocating Nusselt number distributions.

is not apparently shown in Fig. 4(a) for flows with low Reynolds numbers. Thus the coupling *Re–Pu* forces affect heat transfer differently for flows with and without turbulence involved. Nevertheless, in light of the modified axial heat transfer distribution seen in Fig. 4(b) from the stationary results, it suggests the intriguing possibility that the coupled inertial and pulsating forces alter the circulating manner of rib-induced flow cells, and the turbulent flow structures in some way.

Variations of pulsating number can also be achieved by adjusting the frequency at a fixed Reynolds number rather than by varying the Reynolds number at a fixed frequency. The comparisons of the effect of pulsating number in isolation were undertaken for tests where the Reynolds numbers and averaged buoyancy parameters $\beta(T_w - T_b)$ were the same. Fig. 5(a) and (b) show typical variations of the relative Nusselt number ratio, Nu/Nu_0, obtained with four different pulsating number values at Reynolds numbers of 1400 and 3100, respectively. Fig. 5(a) clearly shows the impediment to relative heat transfer, which occurs for pulsating numbers of 4 and 6, and an enhancement in relative heat transfer when the pulsating number is greater than 8. Thus the reciprocating force alone is capable of reducing and enhancing heat transfer at, respectively, low and high pulsating numbers. At high Reynolds numbers ($Re > 3000$), results in the data range of $Pu > 4$ reveal the consistent heat transfer increment when the pulsating number increases; and Fig. 5(b) shows the typical variation. This is thought that, when the relative strength of pulsating force is increased where the turbulence prevails ($Re > 3000$), the flow becomes destabilized, which causes the improved relative heat transfer. Additionally, although the data collected in Fig. 5(a) and (b) shared the same variation range of pulsating numbers, the different relative Nusselt number ratios were obtained at a specific pulsating number (e.g., 4) for flows in low and high Reynolds-number ranges. Thus the relative changes in heat transfer produced by varying the pulsating number are dependent on the Reynolds number. The effects of flow pulsation and convective inertia in this particular ribbing geometry are interactive.

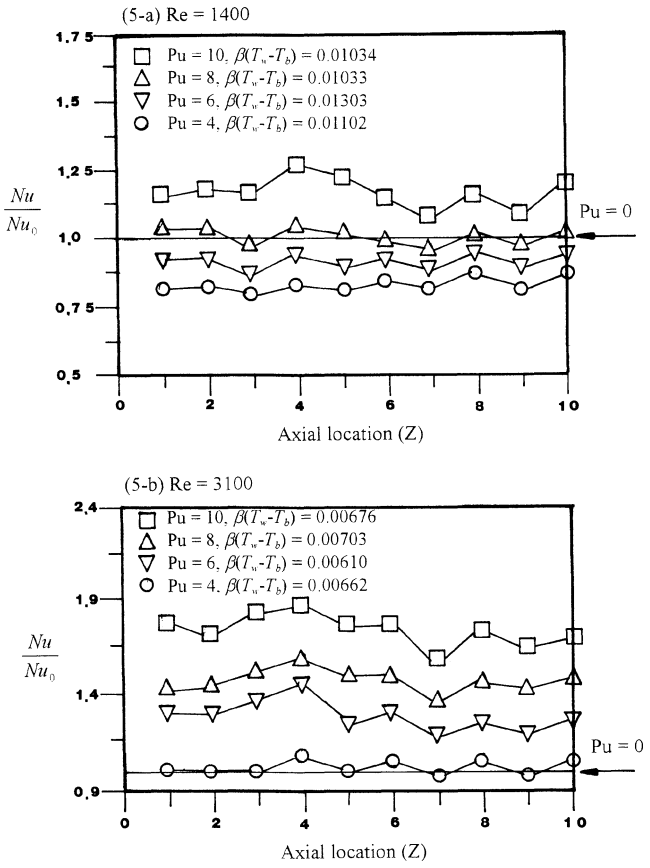

Fig. 5. Axial distributions of relative Nusselt number with Reynolds numbers of 1400 and 3100.

An examination of Reynolds number effect in isolation was performed by comparing the relative Nusselt number data at pulsating number of 6 with Reynolds numbers varying from 1100 to 5312. Fig. 6 shows the typical variations of the relative Nusselt number ratio obtained with five different Reynolds number values. The nominal buoyancy parameter, $\beta(T_w - T_b)$, for this set of data was controlled at 0.007. Because the pulsating number was fixed for each Reynolds number, the relative strength of the reciprocating flow to flow inertia was also fixed by adjusting the reciprocating frequency for the different Reynolds numbers concerned. The data were found to collapse into separate curves of fixed Reynolds numbers. The levels of relative Nusselt number ratio increase with Reynolds number. The influence of flow pulsation at a fixed buoyancy level and pulsating number depends, therefore, on the absolute strength of the inertial force. Higher levels of heat transfer enhancement were found to occur with higher Reynolds numbers.

It has revealed the coupling *Re–Pu* effects on forced convection in this ribbed duct when the buoyancy interaction was controlled at the specific levels. To illustrate the buoyancy effect, the similar approach as to reveal the *Re–Pu* effect described previously was adopted. Tests were performed with fixed Reynolds and pulsating numbers, while the buoyancy number varied systematically. Fig. 7(a)

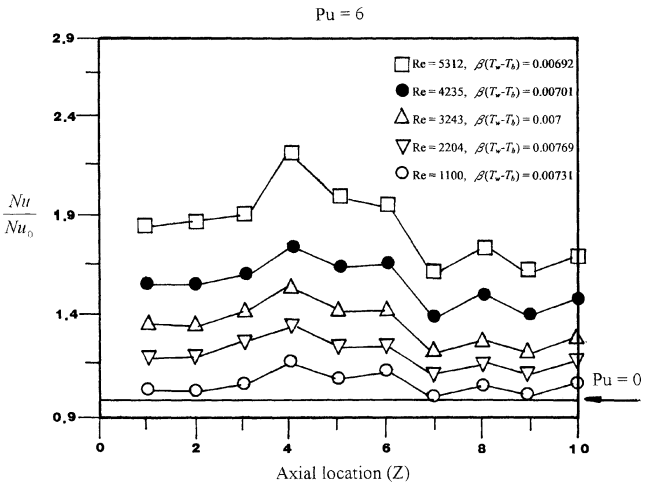

Fig. 6. Axial distributions of relative Nusselt number at fixed pulsating number.

and (b), respectively, show the variations of relative Nusselt number ratio against the buoyancy number for tests undertaken at constant Reynolds or pulsating numbers. All the data points collected from each mid-location have been examined following the manner described in Fig. 7. Note that the Reynolds or pulsating number for each five-point data series shown in Fig. 7(a) or (b) is fixed; and increasing the value of buoyancy parameter, $\beta(T_w - T_b)$, causes the increase of buoyancy number in each data-series. As seen, for a specific Reynolds or pulsating number in each graph of Fig. 7, an increase of buoyancy number creates an overall decrease in the relative Nusselt number ratio. The steeper data series develop at the higher values of pulsating number as shown in Fig. 7(a), and this data trend suggests the enhanced buoyancy effect at the higher pulsating number. However, in Fig. 7(b), the variations of relative Nusselt number ratio at fixed pulsating numbers are not apparently affected by the increase of Reynolds number. In other words, the buoyancy effect is a weak function of Reynolds number.

Note that, in each graph of Fig. 7, the data points of relative Nusselt number ratio at the limiting case with $Bu = 0$ feature the individual *Re* and *Pu* effects on heat transfer, without any buoyancy interaction. These zero buoyancy data were obtained by extrapolating each five-point data series at a specific Reynolds or pulsating number into the zero buoyancy limit through a curve fitting routine. Clearly, the values of these extrapolating data vary with Reynolds and pulsating numbers. Therefore, the individual Reynolds or pulsating number effect without buoyancy interaction was, respectively; pulsating and Reynolds number dependent. Fig. 8 typifies the mutual dependency of the individual Reynolds or pulsating number effect at zero buoyancy condition. As seen in each graph of Fig. 8 for a specific pulsating number, the increase of Reynolds number increases the zero-buoyancy heat transfer level. Using a series of cross plots, based on Fig. 7, but applied to all the *Re*, *Pu* numbers examined, it interpolated a surface of Nusselt number contours at each mid-rib location, which described the variation of

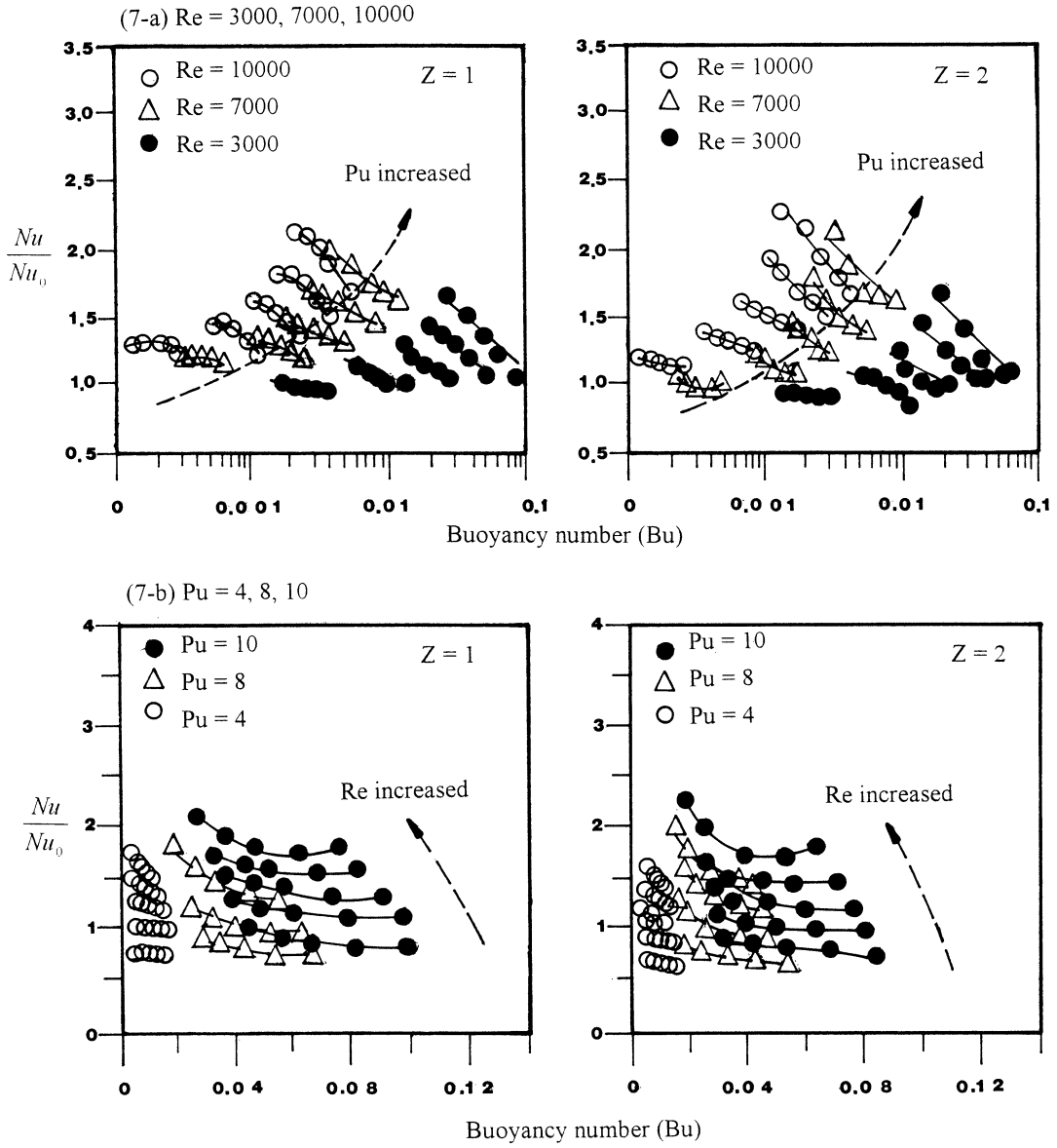

Fig. 7. Effect of reciprocating buoyancy on heat transfer.

zero-buoyancy heat transfer with Reynolds and pulsating numbers. A typical example illustrating the variations of relative Nusselt number ratio with Reynolds and pulsating numbers at zero buoyancy condition is shown in Fig. 9. As shown, with Reynolds number less than 3000, the increase of pulsating number at each specific Reynolds number initially reduces the relative Nusselt number ratio. In this low Reynolds number regime, as the pulsating number is increased to the values above 4, the heat transfer tends to recover with a faster recovering rate at the higher Reynolds number. Heat transfer tends to consistently increase with pulsating number from the stationary duct level in the high Reynolds number regime ($Re > 3000$). Without buoyancy interaction, the nonlinear interaction of convective inertia and reciprocating force follows the contour-map depicted in Fig. 9. These forces create the synergistic, but not the additive, effects on heat transfer in the presence of rib-flows. Nevertheless, within the parametric range tested, the increase of buoyancy level from the zero-buoyancy condition reduces the heat transfer from the baseline references defined in Fig. 9.

As a benchmark heat transfer reference for the design of internal cooling network in a piston, the axially averaged time-mean heat transfer levels for the reciprocating duct are examined. Each spatial-time averaged Nusselt number data was produced by averaging the relative Nusselt number ratios, Nu/Nu_0, collected from all the measured mid-rib locations for a particular set of Reynolds, pulsating and buoyancy numbers tested. Fig. 10 shows the variation of spatial-time averaged Nusselt number ratio, $\overline{Nu}/Nu_0$, with the pulsating number. The spatially averaged buoyancy parameter was selected as 0.00532 for the data collected in Fig. 10. As it has been demonstrated that the *Re*, *Pu* and *Bu* effects are interactive in the reciprocating

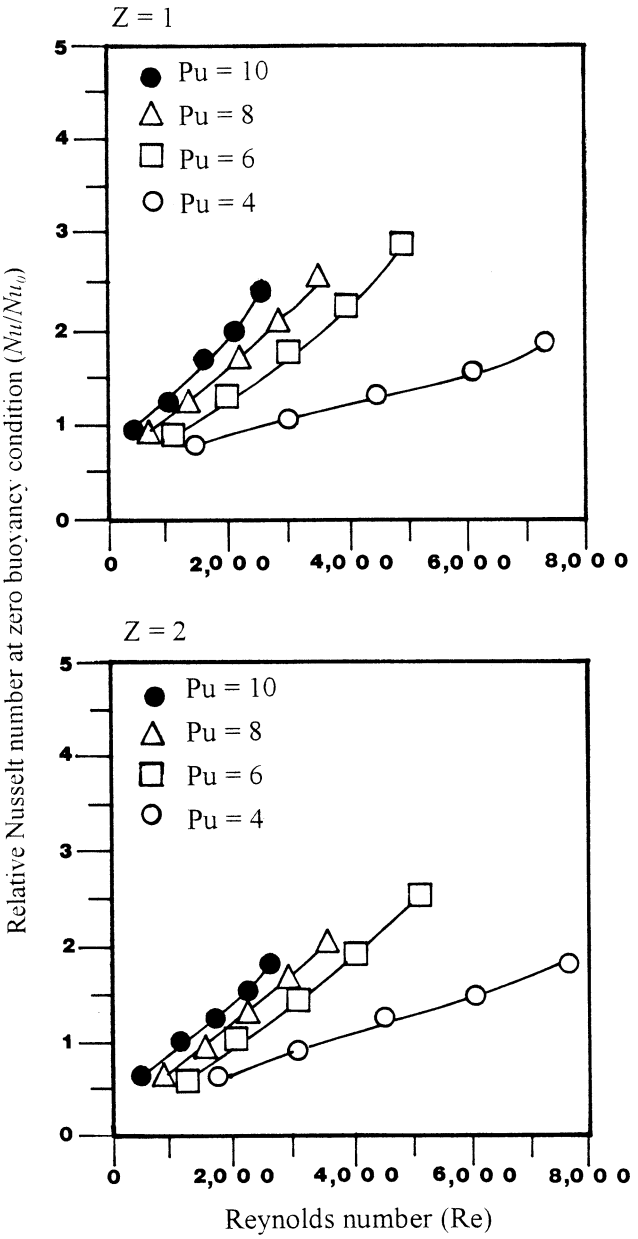

Fig. 8. Extrapolating zero buoyancy heat transfer conditions with various Reynolds and Pulsating numbers.

ribbed duct, the spatial-time averaged Nusselt number ratios collapse into separate lines of fixed Reynolds numbers. With Reynolds numbers of 1200 and 2000, the spatial-time averaged Nusselt number ratio could be reduced to a level about 71% of the stationary value, after which the heat transfer recovery is followed. In the data range with $Re \geqslant 3100$, the spatial-time averaged Nusselt number ratios increase with pulsating number. This increase is enhanced for the data with higher Reynolds number. At a pulsating number of 2.8 and Reynolds number of 10 000, about 130% of heat transfer increments are observed. In general, with flows in the high Reynolds number regime, the overall heat transfer increases with the increase of pulsating number. The derivation of physically consistent empirical formula for assessing the influence of reciprocation on the spatial-time averaged heat transfer is motivated by the need to generate design friendly correlation to aid the evaluation of overall heat transfer in the enhanced cooling passage of piston. The format of correlation has been argued to take the form given by Eq. (1). The asymptotic limit of Eq. (1) with $Re \to 0$ simulates the flow condition that the coolant is trapped in the reciprocating envelope without net through flow. This modifies the present forced convective situation into a closed reciprocating thermosyphon for which the flow and heat transfer physics are created by the vibrational buoyancy [19] rather than the physics described by Eq. (1). With $Re \to \infty$ while the reciprocating frequency remains finite, the pulsating number approaches 0 that is equivalent to the stationary forced convection solution ($\overline{Nu}/Nu_0 = 1$). Led by the observation of all heat flux versions of Fig. 10 and the asymptotic limit of $Re \to \infty$, it is proposed that the empirical correlation could take the possible specific form of

$$\frac{\overline{Nu}}{Nu_0} = 1 + \phi_1 \times Pu + \phi_2 \times Pu^2 \tag{2}$$

where ϕ_1 and ϕ_2 are functions of Reynolds number. With the buoyancy interaction to be absorbed into the coefficients of equations, ϕ_1 and ϕ_2, are correlated as

$$\phi_1 = -0.1644 + 4\text{E}{-5} \times Re \tag{3}$$

$$\phi_2 = 0.0214 - 7.03\text{E}{-6} \times Re + 1.02\text{E}{-9} \times Re^2 \tag{4}$$

Over the entire range of Reynolds number, pulsating number and heat flux level studied, 96% of the experimental Nusselt number ratios, $\overline{Nu}/Nu_0$, were found to agree with ±21% of Eq. (2). Considering the complexity of flow physics involved, the proposed correlation offers an indication of the reciprocating effect on the spatial-time averaged heat transfer. However, the desire to improve the propulsive efficiency of marine Diesel engine by operating at lower engine speeds could lead the cooling channels arranged in a piston to operate with fairly low pulsating number, and impediments to the cooling effectiveness may result from the piston oscillation. Therefore, the reciprocating effect on heat transfer has to be considered in the design stage in order to assure the reliable operation.

4. Conclusions

This experimental study examined the heat transfer physics of forced convection inside a reciprocating square duct fitted with 45° crossed ribs on two opposite walls. The interactive and isolated effects of *Re*, *Pu*, and *Bu* have been particularly studied. In conclusion, the following observations emerge.

(1) As well as a reconfirmation, the stationary Nusselt numbers in a square duct fitted with 45° crossed ribs could be increased up to about 3 and 2.6 times that of the smooth-walled values, respectively, for flows with

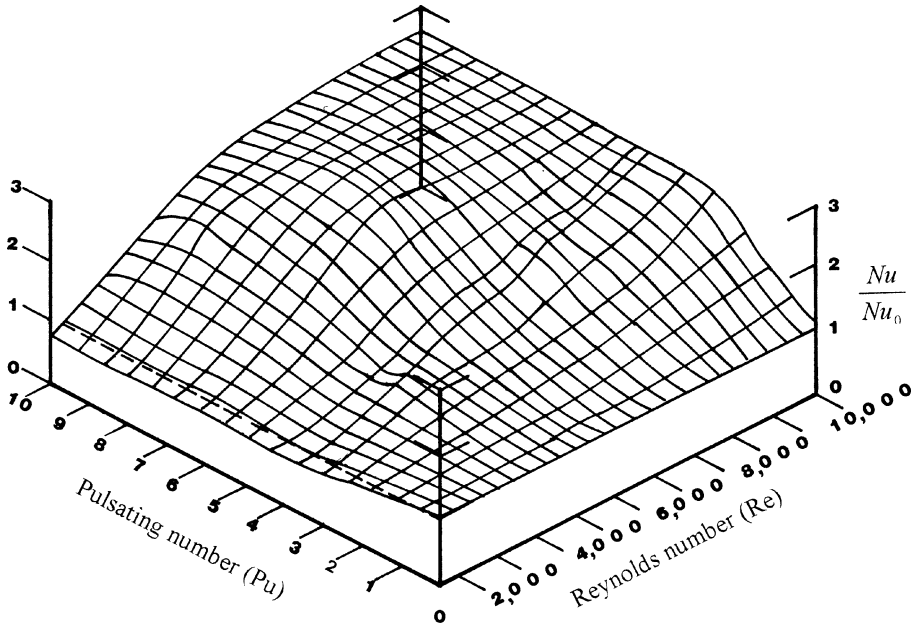

Fig. 9. Reciprocating effect on heat transfer without buoyancy interaction.

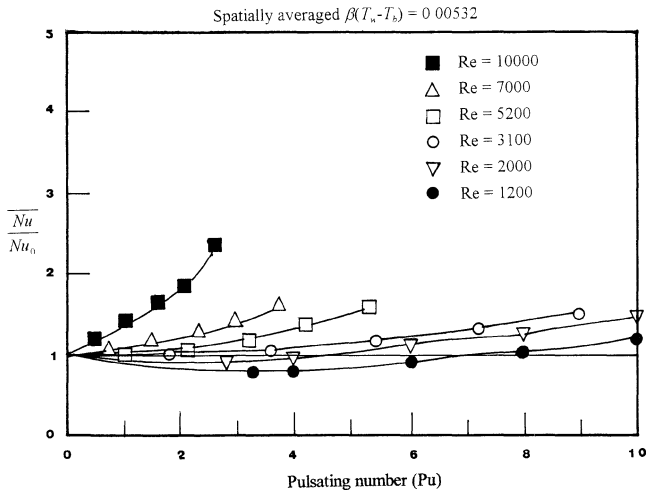

Fig. 10. Variations of spatial-time averaged reciprocating Nusselt number ratio with Reynolds and pulsating numbers.

low and high Reynolds numbers. Buoyancy effect in this stationary ribbed duct is negligible.

(2) The synergistic *Re–Pu* effect that interacts with the rib-induced flows at a specific buoyancy level creates the large-scale wavy-like axial heat transfer distribution with a regular wavelength of two pitches. With $Re < 3000$, the increase of pulsating number at a fixed Reynolds number initially reduces heat transfer. A subsequent heat transfer recovery tendency gradually develops when *Pu* increases. In the high Reynolds number regime ($Re > 3000$), the heat transfer continuously increases with the increase of pulsating number.

(3) The individual Reynolds or pulsating number effect without buoyancy interaction is, respectively; pulsating and Reynolds number dependent. For a specific pulsating number, the increase of Reynolds number increases the zero-buoyancy heat transfer level.

(4) The buoyancy interaction in this reciprocating ribbed duct causes heat transfer reduction. Its effect enhances with pulsating number, but is a weak function of Reynolds number.

(5) The spatial-time averaged Nusselt number ratio could be reduced to a level about 71% of the stationary value with low *Re* and *Pu* numbers. It is therefore essential to ensure that the range of reciprocating flow parameters produced does not create the condition with reduced heat transfer in order to avoid the overheating of an internally cooled piston.

(6) The proposed empirical correlation for the spatial-time averaged heat transfer permits the combined effects of reciprocation and rib-induced flow to be taken into account.

Acknowledgement

This work was funded toward National Kaohsiung Institute of Marine Technology by the National Science Council, Taiwan, ROC under the grant number, NSC 86-2212-E-022-001. Appreciation is given to Mr. M.Y. Ku for his assistance in collecting the experimental data and preparing the graphic drafts.

References

[1] J.C. Han, Y.M. Zhang, C.P. Lee, Augmented heat transfer in square channels with parallel, cross, and V-shaped angled ribs, ASME J. Heat Transfer 113 (1991) 590–596.

[2] M.E. Taslim, T. Li, D.M. Kercher, Experimental heat transfer and friction in channels roughened with angled, V-shaped, and discrete ribs on two opposite walls, ASME J. Turbomachinery 118 (1996) 20–28.
[3] T.M. Liou, J.J. Hwang, Turbulent heat transfer augmentation and friction in periodic fully developed channel flows, ASME J. Heat Transfer 114 (1992) 56–64.
[4] J.R. Shen, Z. Wang, P.T. Ireland, T.V. Jones, A.R. Byerley, Heat transfer enhancement within a turbine blade cooling passage using ribs and combinations of ribs with film cooling holes, ASME J. Turbomachinery 118 (1996) 428–434.
[5] S. Mochizuki, A. Murata, M. Fukunga, Effect of rib arrangements on pressure drop and heat transfer in a rib-roughened channel with a sharp 180 deg turn, ASME J. Turbomachinery 119 (1997) 610–616.
[6] E.P.L. Roberts, M.R. Mackley, The development of asymmetry and period coupling for oscillatory flow in baffled channels, J. Fluid Mech. 328 (1996) 19–48.
[7] A. Okajima, T. Matsumoto, S. Kimura, Aerodynamic characteristics of flat plates with various angles of attack in oscillatory flow, JSME Internat. J. Ser. B 41 (1998) 214–220.
[8] S.W. Chang, L.M. Su, C.C. Hwang, T.L. Yang, Heat transfer in a reciprocating duct fitted with transverse ribs, J. Experimental Heat Transfer 12 (1999) 95–115.
[9] S.W. Chang, L.M. Su, Heat transfer of reciprocating helical tube fitted with full circumferential ribs, Internat. J. Heat Mass Transfer (2001), under printing.
[10] W.D. Morris, R. Salemi, The effects of orthogonal-mode rotation on forced convection in a circular-sectioned tube fitted with full circumferential transverse ribs, in: AGARD Conf. Proc., Turkey, October 1992, pp. 527–538, Paper 11.
[11] S. Fann, W.J. Yang, N. Zhang, Local heat transfer in a rotating serpentine passage with rib-roughened surfaces, Internat. J. Heat Mass Transfer 37 (1994) 217–228.
[12] B.V. Johnson, J.H. Wagner, G.D. Steuber, F.C. Yeh, Heat transfer in rotating serpentine passages with trips skewed to the flow, ASME J. Turbomachinery 116 (1994) 113–123.
[13] A.R. Holowenko, Dynamics of Machinery, Wiley, New York, 1955, pp. 238–241.
[14] B.Z. Pu, Yang, Johnson, Advanced Heat Transfer, Shanghai Traffic University Press, 1996, ISBN7-313-01615-8, pp. 51–55 (in Chinese).
[15] Editorial Board of ASME J. Heat Transfer (1993); J. Heat Transfer Policy on reporting uncertainties in experimental measurements and results; ASME J. Heat Transfer, 115, pp. 5–6.
[16] W.M. Kays, M.E. Crawford, Convective Heat and Mass Transfer, 2nd edn., McGraw-Hill, New York, 1980.
[17] F.W. Dittus, L.M.K. Boelter, University of California, Berkeley, CA, Publications in Engineering, Vol. 2 (1930), p. 443.
[18] R. Siegel, Influence of oscillation-induced diffusion on heat transfer in a uniformly heated channel, ASME J. Heat Transfer 109 (1987) 244–247.
[19] G.Z. Gershuni, D.V. Lyubimov, Thermal Vibrational Convection, Wiley, New York, 1997, ISBN 0-471-97385-8.